Available online at www.sciencedirect.com
ScienceDirect
Comput. Methods Appl. Mech. Engrg. 196 (2007) 4779–4788
Computer methods in applied mechanics and engineering
www.elsevier.com/locate/cma

Phase field computations for ternary fluid flows

Junseok Kim

Department of Mathematics, Dongguk University, Seoul 100-715, Republic of Korea

Received 8 February 2007; received in revised form 20 June 2007; accepted 24 June 2007
Available online 19 July 2007

Abstract

We present a new phase field model for three-component immiscible liquid flows with surface tension. In the phase field approach, the classical sharp-interface between the two immiscible fluids is replaced by a transition region across which the properties of fluids change continuously. The proposed method incorporates a chemical potential which can eliminate the unphysical phase field profile and a continuous surface tension force formulation from which we can calculate the pressure field directly from the governing equations. The capabilities of the method are demonstrated with several examples. We compute the ternary phase separation via spinodal decomposition, equilibrium phase field profiles, pressure field distribution, and a three-interface contact angle resulting from a spreading liquid lens on an interface. The numerical results show excellent agreement with analytical solutions.

Keywords: Continuum surface tension; Phase field model; Navier–Stokes equation; Ternary Cahn–Hilliard equation; Interfacial tension; Nonlinear multigrid method

1. Introduction

Many biomedical, chemical, and industrial processes involve mixtures of three or more liquids. For example, mixing two immiscible fluids produces an emulsion, which is defined as a dispersion of droplets of one fluid in a second fluid. Double emulsions are highly structured fluids consisting of emulsion drops that contain smaller droplets inside [35]. Emulsions play critical roles in many forms of applications such as prolonged drug delivery systems [7], entrapment of vitamin [3], and flavor encapsulation for food additives [12].

There have been few theoretical and numerical studies of flows containing three liquid components [5,22,29] as compared to a large body of research on two-phase fluid flows. For example, the volume-of-fluid (VOF) [15,16,26,33], level set method [9,27,30,32], immersed boundary method [14], and phase field method [2,10] are used for the studies of two-component flow. See a recent review paper [23] for more details of two-phase fluid flows. In this paper, we present our study of a phase field model for the mixture of three immiscible fluids. Here we view the phase field model as a computational method. Our model for surface tension effect is different from thermodynamically derived ones [1]. We take continuum surface tension (CSF) framework [6] to model surface tension effects in our phase-field model for three-component fluids. There is another phase-field approach which is based on an ensemble averaging. Based on a superposition of microscopic and macroscopic interface morphologies, an expression for the interfacial momentum source due to surface tension is introduced that is equivalent to the capillary stress term encountered in thermodynamically derived models [31]. The most significant computational advantage of this method is that explicit tracking of the interface is unnecessary.

We propose a ternary phase field model which combines good features of previous multiphase models [5,20]. First, we use the continuous surface tension formulation for phase field models, from which the pressure field can be calculated directly from the governing equations. Second, we use a non-constant Lagrange-multiplier in the chemical potential term, which guarantees that non-physical

E-mail address: cfdkim@dongguk.edu
URL: http://math.uci.edu/~jskim/

0045-7825/$ - see front matter © 2007 Elsevier B.V. All rights reserved.
doi:10.1016/j.cma.2007.06.016

apparition of one phase inside the interface between the other two phases will not occur. The primary advantage of the continuous surface tension formulation for ternary fluid flows is that it allows us to extend three-component fluid flow model to an arbitrary number of fluid components (more than three components, e.g., four-component fluid flow) [21].

The remaining parts of this paper are organized as follows. In Section 2, we describe a phase field model for the mixture of three immiscible fluids. In Section 3, we give a numerical solution. Representative numerical experiments for ternary fluid flow are provided in Section 4. In Section 5, conclusions are drawn.

2. A phase field model for the mixture of three immiscible fluids

We consider viscous three-component incompressible fluid flow with surface tension. The fluid dynamics are described by the Navier–Stokes equations with surface tension force:

$$\rho\left(\frac{\partial \mathbf{u}}{\partial t}+\mathbf{u}\cdot\nabla\mathbf{u}\right)=-\nabla p+\nabla\cdot[\eta(\nabla\mathbf{u}+\nabla\mathbf{u}^{\mathrm{T}})]+\mathbf{SF}+\rho\mathbf{g},$$
$$\nabla\cdot\mathbf{u}=0,$$

where ρ is the fluid density, $\mathbf{u}$ is the fluid velocity, p is the pressure, η is the fluid viscosity, and $\mathbf{SF}$ is the surface tension of the interface. Density and viscosity are constant in each phase but may vary from phase to phase taking values ρ_i and η_i in phase i. The Navier–Stokes equations without the surface tension term are applied for each phase of the flow away from the interface [23]. The composition of a ternary mixture (A, B, and C) can be mapped onto an equilateral triangle (the Gibbs triangle [25]) whose corners represent 100% concentration of A, B or C as shown in Fig. 1. Mixtures with components lying on lines parallel to $\overline{BC}$ contain the same percentage of A; those with lines parallel to $\overline{AC}$ have the same percentage of B concentration; and analogously for the C concentration. In Fig. 1, the mixture at the position marked '$\circ$' contains 30% A, 60% B, and 10% C.

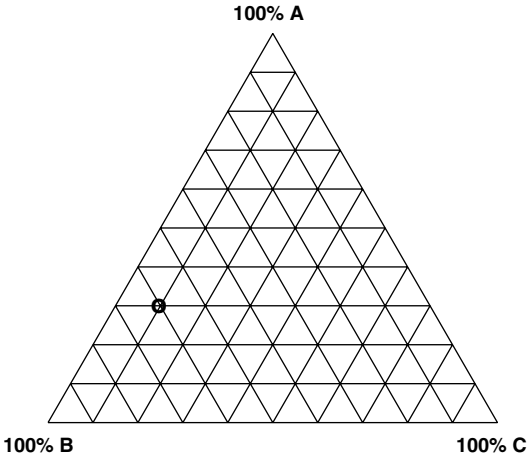

Fig. 1. Gibbs triangle. At the top corner $c_1=1, c_2=0, c_3=0$, at the left corner $c_1=0, c_2=1, c_3=0$, and at the right corner $c_1=0, c_2=0, c_3=1$. At the position marked '$\circ$', $c_1=0.3$, $c_2=0.6$, and $c_3=0.1$.

Clearly the total percentage must sum to 100%, or expressed as a mole fraction, $c_1+c_2+c_3=1$, so that, admissible states will belong to the Gibbs triangle

$$\mathrm{GT}:=\left\{(c_1,c_2,c_3)\in\mathbb{R}^3\middle|\sum_{i=1}^{3}c_i=1,\ 0\leqslant c_i\leqslant 1\right\}.$$

We postulate that the free energy can be written as follows:

$$\mathscr{F}=\int_\Omega\left[F(c_1,c_2,c_3)+\frac{\epsilon^2}{2}\sum_{i=1}^{3}|\nabla c_i|^2\right]\mathrm{d}\mathbf{x},\tag{1}$$

where $F(c_1,c_2,c_3)=\frac{1}{4}\sum_{i=1}^{3}c_i^2(1-c_i)^2$ and Ω is an open, bounded subset of $\mathbb{R}^n(n=1,2,3)$ occupied by the system. The time dependence of c_i is given by the following advective Cahn–Hilliard equation for describing each phase convection:

$$\frac{\partial c_i}{\partial t}+\mathbf{u}\cdot\nabla c_i=\nabla\cdot(M\nabla\mu_i),\quad i=1,2,3,\tag{2}$$

$$\mu_i=\frac{\partial F(c_1,c_2,c_3)}{\partial c_i}-\epsilon^2\Delta c_i+\beta(c_1,c_2,c_3),\tag{3}$$

where M is a mobility, ϵ is a positive constant, and $\beta(c_1,c_2,c_3)$ is a non-constant Lagrange-multiplier, which is enforcing that the sum of the variational derivatives is zero, i.e., $\sum_{i=1}^{3}\mu_i=0$ [17]. The natural and mass conserving boundary conditions for the quaternary CH system are the zero Neumann boundary ones:

$$\nabla c_i\cdot\mathbf{n}=\nabla\mu_i\cdot\mathbf{n}=0\quad\text{on }\partial\Omega,\tag{4}$$

where $\mathbf{n}$ is the unit normal vector to $\partial\Omega$. To calculate $\beta(c_1,c_2,c_3)$, we sum up Eqs. (2) and (3) and write the equation satisfied by $S=c_1+c_2+c_3$,

$$\frac{\partial S}{\partial t}+\mathbf{u}\cdot\nabla S=\nabla\cdot\left[M\nabla\left(\sum_{i=1}^{3}\frac{\partial F}{\partial c_i}-\epsilon^2\Delta S+3\beta(c_1,c_2,c_3)\right)\right].\tag{5}$$

We want $S\equiv 1$ to be a solution to this Eq. (5). Therefore, $\beta(c_1,c_2,c_3)=-\frac{1}{3}\sum_{i=1}^{3}\frac{\partial F}{\partial c_i}$. For the sake of simplicity, we assume that each component of the fluids has the same mass density and the mobility M is constant. Since $c_1+c_2+c_3=1$ for ternary systems, we only need to solve the equations with c_1 and c_2. Let $\mathbf{c}=(c_1,c_2)$ and $\boldsymbol{\mu}=(\mu_1,\mu_2)$, then the three-component fluids are governed by the modified Navier–Stokes equations and the convective Cahn–Hilliard equations.

$$\rho(\mathbf{c})\left(\frac{\partial \mathbf{u}}{\partial t}+\mathbf{u}\cdot\nabla\mathbf{u}\right)=-\nabla p+\nabla\cdot[\eta(\mathbf{c})(\nabla\mathbf{u}+\nabla\mathbf{u}^{\mathrm{T}})]+\mathbf{SF}, \tag{6}$$

$$\nabla\cdot\mathbf{u}=0, \tag{7}$$

$$\frac{\partial \mathbf{c}}{\partial t}+\mathbf{u}\cdot\nabla\mathbf{c}=M\Delta\boldsymbol{\mu}, \tag{8}$$

$$\boldsymbol{\mu}=\mathbf{f}(\mathbf{c})-\epsilon^2\Delta\mathbf{c}, \tag{9}$$

where the variable density and the viscosity are given as

$$\begin{aligned}\rho(\mathbf{c})&=\rho_1c_1+\rho_2c_2+\rho_3(1-c_1-c_2),\\ \eta(\mathbf{c})&=\eta_1c_1+\eta_2c_2+\eta_3(1-c_1-c_2),\\ \mathbf{f}(\mathbf{c})&=(f_1(\mathbf{c}),f_2(\mathbf{c}))\\ &=(c_1^3-1.5c_1^2+0.5c_1-c_1c_2(1-c_1-c_2),\\ &\quad c_2^3-1.5c_2^2+0.5c_2-c_1c_2(1-c_1-c_2)).\end{aligned}$$

The interfacial tension force **SF** acts in a normal direction to the fluid interface and is proportional to the curvature times a surface tension coefficient. Therefore, the capillary term can be written in the form

$$\mathbf{SF}=-\sum_{i=1}^{3}\alpha\epsilon\gamma_i\nabla\cdot\left(\frac{\nabla c_i}{|\nabla c_i|}\right)|\nabla c_i|\nabla c_i,$$

where γ_i is the phase specific surface tension coefficient and satisfies the relation, $\sigma_{ij}=\gamma_i+\gamma_j$ [29]. σ_{ij} are the physical fluid surface tension coefficients between the fluid i and the fluid j (see Fig. 2). The decomposition is uniquely defined. That is, $\gamma_1=(\sigma_{12}-\sigma_{23}+\sigma_{13})/2$, $\gamma_2=(\sigma_{12}+\sigma_{23}-\sigma_{13})/2$, and $\gamma_3=(-\sigma_{12}+\sigma_{23}+\sigma_{13})/2$. To match the surface tension of the sharp-interface model, α must satisfy

$$\int_{-\infty}^{\infty}\alpha\epsilon|\nabla c_1^{\mathrm{eq}}(x,y)|^2\,\mathrm{d}x=1, \tag{10}$$

where $c_1^{\mathrm{eq}}(x,y)=\left[1+\tanh\left(x/\left(2\sqrt{2}\epsilon\right)\right)\right]/2$ is an equilibrium composition profile in the infinite domain, $\Omega=(-\infty,\infty)\times(-\infty,\infty)$, when the chemical potential is given as Eq. (9) with $c_3(x,y)\equiv 0$ [5,19]. It is a good approximation in the finite domain since it approaches 0 or 1 away from the interfacial transition zone. Therefore from Eq. (10), we get $\alpha=6\sqrt{2}$. To make the governing equations dimensionless, we choose the following definitions:

$$\begin{aligned}&\mathbf{x}'=\frac{1}{L}\mathbf{x},\quad \mathbf{u}'=\frac{1}{U}\mathbf{u},\quad t'=\frac{U}{L}t,\quad \rho'=\frac{\rho}{\rho_1},\\ &p'=\frac{p}{\rho_1U^2},\quad \eta'=\frac{\eta}{\eta_1},\end{aligned} \tag{11}$$

where the primed quantities are dimensionless and L, U, ρ_1, η_1 are, respectively, the characteristic length, characteristic velocity, the density of fluid 1, and the dynamic viscosity of fluid 1. Substituting the above Eqs. (11) into Eqs. (6)–(9), and dropping the primes, we have

$$\frac{\partial \mathbf{u}}{\partial t}+\mathbf{u}\cdot\nabla\mathbf{u}=-\nabla p+\frac{1}{Re}\nabla\cdot[\eta(\mathbf{c})(\nabla\mathbf{u}+\nabla\mathbf{u}^{\mathrm{T}})]+\mathbf{SF}, \tag{12}$$

$$\nabla\cdot\mathbf{u}=0, \tag{13}$$

$$\frac{\partial \mathbf{c}}{\partial t}+\mathbf{u}\cdot\nabla\mathbf{c}=\frac{1}{Pe}\Delta\boldsymbol{\mu}, \tag{14}$$

$$\boldsymbol{\mu}=\mathbf{f}(\mathbf{c})-\epsilon^2\Delta\mathbf{c}, \tag{15}$$

where ϵ is redefined according to the scaling and

$$\mathbf{SF}=-\sum_{i=1}^{3}\frac{6\sqrt{2}\epsilon}{We_i}\nabla\cdot\left(\frac{\nabla c_i}{|\nabla c_i|}\right)|\nabla c_i|\nabla c_i.$$

The dimensionless parameters are the Reynolds number, $Re=\rho_1UL/\eta_1$, the phase specific Weber number, $We_i=\rho_1LU^2/\gamma_i$, and the diffusional Peclet number, $Pe=LU/(M\mu_*)$. Pe measures the relative strengths of advection and diffusion. $\epsilon>0$ is a non-dimensional measure of non-locality resulting from the gradient energy (Cahn number) and introduces an internal length scale (interface thickness).

The key difference between these Eqs. (6)–(9) and the previous phase field models [5,22] is the presence of the new surface tension force formulation which was applied to the two-component fluid flow model [20]. The presence of this term allows these equations to be applied over an arbitrary number of component fluid flow models [21].

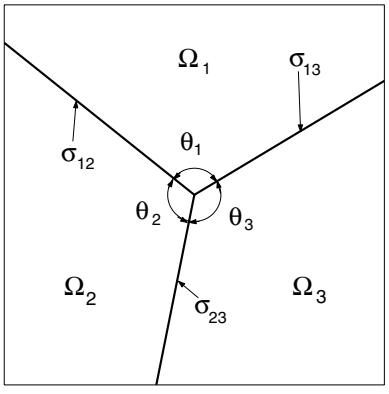

Fig. 2. Schematic of domain. σ_{ij} denotes the surface tension coefficient of fluids 'i' and 'j'. θ_i is a contact angle of phase i with two other phases.

3. Numerical solution

An efficient approximation can be obtained by decoupling the solution of the momentum equations from the solution of the continuity equation by a projection method [8]. The extension to 3D is straightforward. We will focus on describing the idea in two-dimensions.

A staggered marker-and-cell (MAC) mesh of Harlow and Welch [18] is used in which pressure and phase fields are stored at cell centers and velocities at cell interfaces (see Fig. 3). Let a computational domain be partitioned in Cartesian geometry into a uniform mesh with mesh spacing h.

At the beginning of each time step, given $\mathbf{u}^n$, and $\mathbf{c}^n$, we want to find $\mathbf{u}^{n+1}$, $\mathbf{c}^{n+1}$, and p^{n+1} which solve the following temporal discretization of Eqs. (12)–(15) of motion:

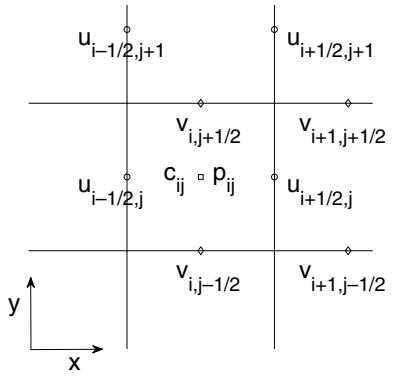

Fig. 3. Velocities are defined at cell boundaries while the pressure and phase field are defined at the cell centers, Ω_{ij}.

$$\frac{\mathbf{u}^{n+1}-\mathbf{u}^n}{\Delta t} = -\nabla_d p^{n+1} + \frac{1}{Re}\nabla_d \cdot \eta(\mathbf{c}^n)[\nabla_d \mathbf{u}^n + (\nabla_d \mathbf{u}^n)^{\mathrm{T}}] + \mathbf{SF}^n - (\mathbf{u}\cdot\nabla_d \mathbf{u})^n, \tag{16}$$

$$\nabla_d \cdot \mathbf{u}^{n+1} = 0, \tag{17}$$

$$\frac{\mathbf{c}^{n+1}-\mathbf{c}^n}{\Delta t} = \frac{1}{Pe}\Delta_d \boldsymbol{\mu}^{n+\frac{1}{2}} - (\mathbf{u}\cdot\nabla_d \mathbf{c})^n, \tag{18}$$

$$\boldsymbol{\mu}^{n+\frac{1}{2}} = \frac{1}{2}[\mathbf{f}(\mathbf{c}^n) + \mathbf{f}(\mathbf{c}^{n+1})] - \frac{1}{2}\epsilon^2 \Delta_d(\mathbf{c}^n + \mathbf{c}^{n+1}). \tag{19}$$

The outline of the main procedures in one time step is:

Step 1. Initialize $\mathbf{c}^0$ to be the locally equilibrated concentration profile and $\mathbf{u}^0$ to be the divergence-free velocity field.

Step 2. Solve an intermediate velocity field, $\tilde{\mathbf{u}}$, which does not satisfy the incompressible condition, without the pressure gradient term,

$$\frac{\tilde{\mathbf{u}}-\mathbf{u}^n}{\Delta t} = \frac{1}{Re}\nabla_d \cdot \eta(\mathbf{c}^n)[\nabla_d \mathbf{u}^n + (\nabla_d \mathbf{u}^n)^{\mathrm{T}}] - \mathbf{u}^n \cdot \nabla_d \mathbf{u}^n + \mathbf{SF}^n,$$

where the convective term, $\mathbf{u}^n \cdot \nabla_d \mathbf{u}^n$, is computed using a higher order ENO procedure derived in Ref. [28]. The surface tension force term, $\mathbf{SF}^n$, is described in Section 3.1. Then, we solve the following equations for the advanced pressure field at $(n+1)$ time step.

$$\frac{\mathbf{u}^{n+1}-\tilde{\mathbf{u}}}{\Delta t} = -\nabla_d p^{n+1}, \tag{20}$$

$$\nabla_d \cdot \mathbf{u}^{n+1} = 0. \tag{21}$$

With application of the divergence operator to Eq. (20), we find that the Poisson equation for the pressure at the advanced time $(n+1)$.

$$\Delta_d p^{n+1} = \frac{1}{\Delta t}\nabla_d \cdot \tilde{\mathbf{u}}, \tag{22}$$

where we have made use of Eq. (21). The resulting linear system of Eq. (22) is solved using a multigrid method, specifically, V-cycles with a Gauss–Seidel relaxation. Then the divergence-free velocities are defined by $\mathbf{u}^{n+1} = \tilde{\mathbf{u}} - p^{n+1}$.

Step 3. Update the phase field $\mathbf{c}^n$ to $\mathbf{c}^{n+1}$. This step is described in Appendix A. These complete the one time step.

3.1. Discretization of the surface tension force formulation

In this section, we derive a discretization of the cell-face based surface tension force. Let ϕ be one of three phase fields, c_1, c_2, and c_3. A normal vector at the top right vertex of a computational cell Ω_{ij} is given by

$$\mathbf{n}_{i+\frac{1}{2},j+\frac{1}{2}} = \left(n^x_{i+\frac{1}{2},j+\frac{1}{2}}, n^y_{i+\frac{1}{2},j+\frac{1}{2}}\right) = \left(\frac{\phi_{i+1,j}+\phi_{i+1,j+1}-\phi_{ij}-\phi_{i,j+1}}{2h}, \frac{\phi_{i,j+1}+\phi_{i+1,j+1}-\phi_{ij}-\phi_{i+1,j}}{2h}\right).$$

The curvature $\kappa(\phi_{ij})$ is given by

$$\kappa(\phi_{ij}) = \nabla_d \cdot \left(\frac{\mathbf{n}}{|\mathbf{n}|}\right)_{ij} = \frac{1}{2h}\left(\frac{n^x_{i+\frac{1}{2},j+\frac{1}{2}} + n^y_{i+\frac{1}{2},j+\frac{1}{2}}}{|\mathbf{n}_{i+\frac{1}{2},j+\frac{1}{2}}|} + \frac{n^x_{i+\frac{1}{2},j-\frac{1}{2}} - n^y_{i+\frac{1}{2},j-\frac{1}{2}}}{|\mathbf{n}_{i+\frac{1}{2},j-\frac{1}{2}}|} - \frac{n^x_{i-\frac{1}{2},j+\frac{1}{2}} - n^y_{i-\frac{1}{2},j+\frac{1}{2}}}{|\mathbf{n}_{i-\frac{1}{2},j+\frac{1}{2}}|} - \frac{n^x_{i-\frac{1}{2},j-\frac{1}{2}} + n^y_{i-\frac{1}{2},j-\frac{1}{2}}}{|\mathbf{n}_{i-\frac{1}{2},j-\frac{1}{2}}|}\right).$$

The cell-centered normal is the average of the vertex normals,

$$\nabla_d \phi_{ij} = \left(\mathbf{n}_{i+\frac{1}{2},j+\frac{1}{2}} + \mathbf{n}_{i+\frac{1}{2},j-\frac{1}{2}} + \mathbf{n}_{i-\frac{1}{2},j+\frac{1}{2}} + \mathbf{n}_{i-\frac{1}{2},j-\frac{1}{2}}\right)/4.$$

Let $(sf^x_{ij}(\phi), sf^y_{ij}(\phi)) = \kappa(\phi_{ij})|\nabla_d \phi_{ij}|\nabla_d \phi_{ij}$. Then, the required face-centered values are obtained by interpolating from the two nearest cell-centered values,

$$SF^{x-edge}_{i+\frac{1}{2},j}(\mathbf{c}) = -\sum_{k=1}^{3}\frac{3\sqrt{2}\epsilon}{We_k}(sf^x_{ij}(c_k) + sf^x_{i+1,j}(c_k)) \quad \text{and}$$

$$SF^{y-edge}_{i,j+\frac{1}{2}}(\mathbf{c}) = -\sum_{k=1}^{3}\frac{3\sqrt{2}\epsilon}{We_k}(sf^y_{ij}(c_k) + sf^y_{i,j+1}(c_k)).$$

4. Computational verification of the model

We now present numerical results for several standard problems with a three-component mixture to illustrate the flexibility and accuracy of the new phase field model for ternary immiscible fluid flows. The numerical experiments are the spinodal decomposition dynamics in a ternary mixture with a spatially varying mobility, equilibrium phase field profiles with two different chemical potentials, the pressure field distribution, and the contact angle of a liquid lens located at an interface between two other immiscible fluids.

4.1. Spinodal decomposition – phase separation

We begin the numerical experiments with an example of spinodal decomposition of a ternary mixture. When a one-

phase homogeneous system composed of three species, at high temperature and thermal equilibrium, is rapidly cooled to a uniform temperature below a critical temperature, where it is unstable with respect to concentration fluctuations, spinodal decomposition takes place. The system separates into spatial regions rich in one phase and poor in the other phases and evolves into an equilibrium state with lower overall free energy [13]. Ternary spinodal decomposition has been studied numerically by [4,11,13,24]. We use the ternary Cahn–Hilliard system, (2) and (3) with zero velocity, $\mathbf{u} = 0$. In the simulations, the initial conditions were random perturbations of the maximum amplitude 0.05 of the uniform state $\mathbf{c} = \mathbf{c}_{\text{ave}} = (1/3, 1/3)$. A 256×256 mesh was used on the square domain $\Omega = [1] \times [0, 1]$ for the spatial discretization and a time step, $\Delta t = 0.1/512$ was employed for the time integration. We took a spatially varying mobility, $M = M(x, y) = 0.01 + 0.99y$ and $\epsilon = 0.0035$.

The result is presented in Fig. 4. The area shown by white indicates the C phase region; while the gray and black color regions stand for A-rich and B-rich domains, respectively. We observed three phases in the early stages of spinodal decomposition. Since the composition was completely symmetric with respect to the three components, all three phases had similar morphologies and evolution dynamics [11]. As we can expect from the form of the mobility, at an earlier time Fig. 4a and a later time Fig. 4b, computations show non-uniform coarsening wherein the smaller (larger) scales occur in the lower (upper) regions.

4.2. Comparison between two different chemical potentials – equilibrium phase field profiles

The computational domain was 2×1. We used a uniform grid of 128×64. The initial conditions were

$$c_1(x, y, 0) = 0.5\left(1 - \tanh\left(\frac{\sqrt{(x-0.5)^2 + (y-0.5)^2} - 0.15}{2\sqrt{2}\epsilon}\right)\right), \tag{23}$$

$$c_2(x, y, 0) = 0.5\left(1 - \tanh\left(\frac{\sqrt{(x-1.5)^2 + (y-0.5)^2} - 0.15}{2\sqrt{2}\epsilon}\right)\right). \tag{24}$$

The simulations were stopped when profiles did not change for a long time. The dependence of the numerical solution on the chemical potential is demonstrated in Figs. 5a and b.

In Fig. 5a, we show the numerical equilibrium profiles of c_1, c_2, and c_3 with the previous chemical potential [22]. The phase c_1 appeared between the phase c_2 and c_3 interface, which was not a physical phenomenon. Likewise, the phase c_2 appeared between the phase c_1 and c_3 interface. Fig. 5b shows the numerical equilibrium profiles of c_1, c_2, and c_3 with the current chemical potential, $\boldsymbol{\mu} = (c_1^3 - 1.5c_1^2 + 0.5c_1 - c_1c_2(1 - c_1 - c_2) - \epsilon^2\Delta c_1, \quad c_2^3 - 1.5c_2^2 + 0.5c_2 - c_1c_2(1 - c_1 - c_2) - \epsilon^2\Delta c_2)$. We noticed very small changes in the numerically equilibrated c_1, c_2, and c_3 compared to the initial profiles, Eqs. (23) and (24).

In Fig. 6, we show slices of the phase fields at $y = 0.5$. In Fig. 6a, note that there were non-physical phase profiles in other phase boundaries. In Fig. 6b, note that there were no non-physical phase profiles in other phase boundaries.

4.3. Pressure field distribution – refinement study

To demonstrate the ability to calculate the pressure field directly from the governing equations using the present

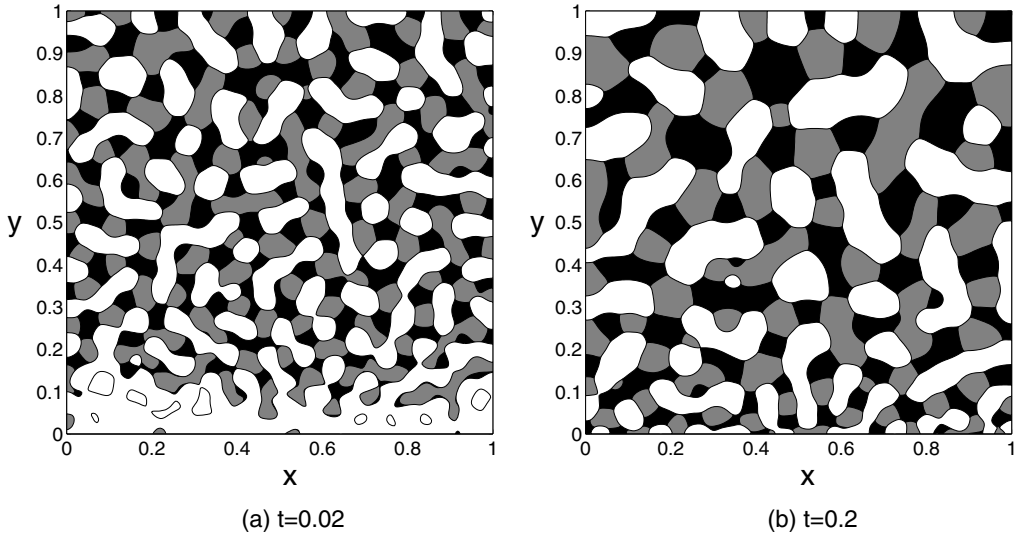

Fig. 4. The temporal evolution of morphologies during a spinodal phase separation of a ternary system with average composition $\mathbf{c}_{\text{ave}} = (1/3, 1/3)$. Phase A is represented by the gray region, phase B by the black region, and phase C by the white region.

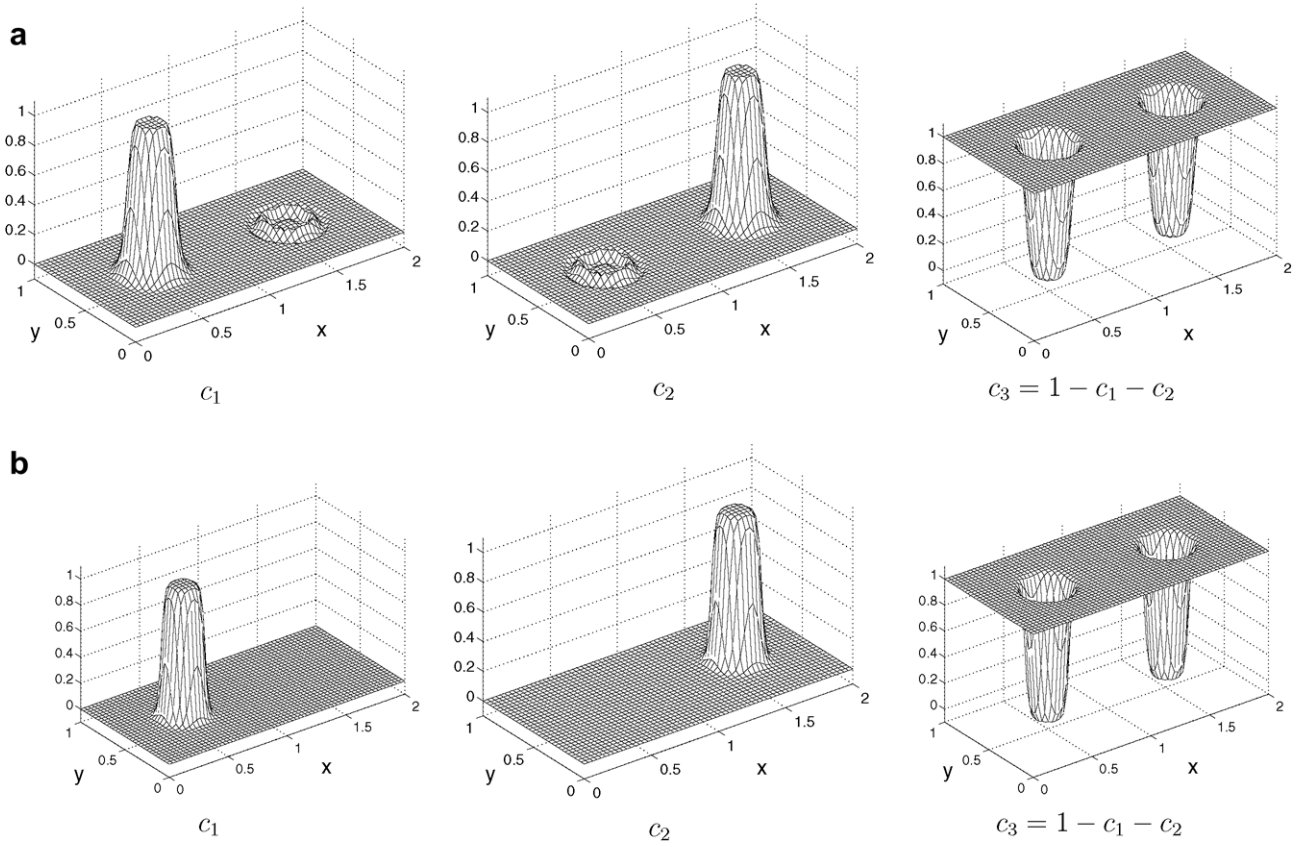

Fig. 5. (a) The equilibrium state obtained with the previous chemical potential [22]. (b) The equilibrium state obtained with the current chemical potential, $\boldsymbol{\mu} = (c_1^3 - 1.5c_1^2 + 0.5c_1 - c_1c_2(1 - c_1 - c_2) - \epsilon^2\Delta c_1,\ c_2^3 - 1.5c_2^2 + 0.5c_2 - c_1c_2(1 - c_1 - c_2) - \epsilon^2\Delta c_2)$.

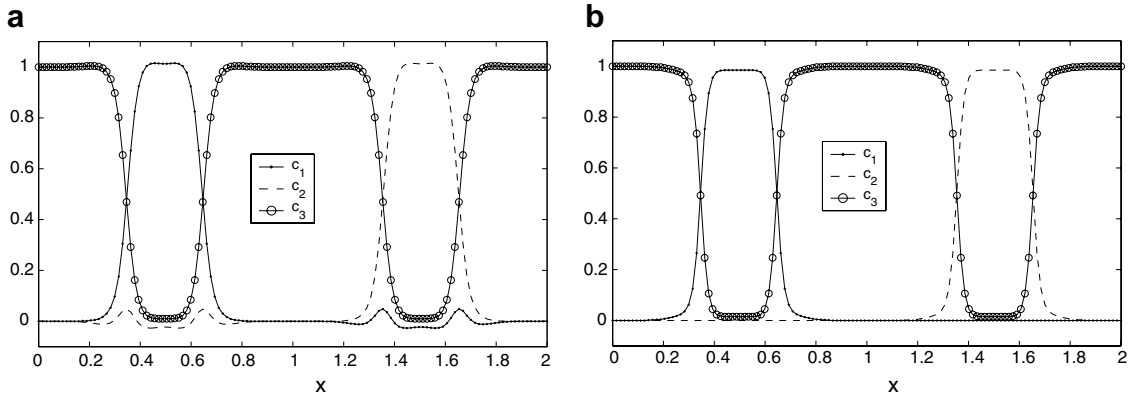

Fig. 6. Vertical cutline of phase fields at $y = 0.5$ with the previous chemical potential (a) and the current chemical potential (b).

model, we considered the equilibrium of two drops placed within another fluid. In the absence of viscous, gravitational, and other external forces, surface tension caused a static liquid drop to become spherical. The Laplace formula [6] for an infinite cylinder surrounded by a background fluid at zero pressure gives $p_{\text{drop}} = \sigma\kappa = \sigma/R$, where p_{drop} is the drop pressure, σ is the surface tension coefficient, κ is the curvature, and R is the drop radius. In this test, we selected the same initial condition for c_1 and c_2 as before, Eqs. (23) and (24) sketched in Fig. 7a. We solved the following Eq. (25) on the computational domain, $\Omega = [0,2]\times[0,1]$. The drop radius $R = 0.15, \sigma_{13} = 0.075, \sigma_{23} = 0.15$, and $\sigma_{12} = 1$ are used. The pressure field is shown in Fig. 7b.

$$\Delta p = \nabla \cdot \mathbf{SF}. \tag{25}$$

The convergence of the CFS model to the theory was demonstrated by the results shown in Fig. 7c for the drop pressure computed with recursively refined meshes (256×128, 512×256, and 1024×512). Increasing resolution localized the surface forces and yielded a uniform ring around the circumference of the drop.

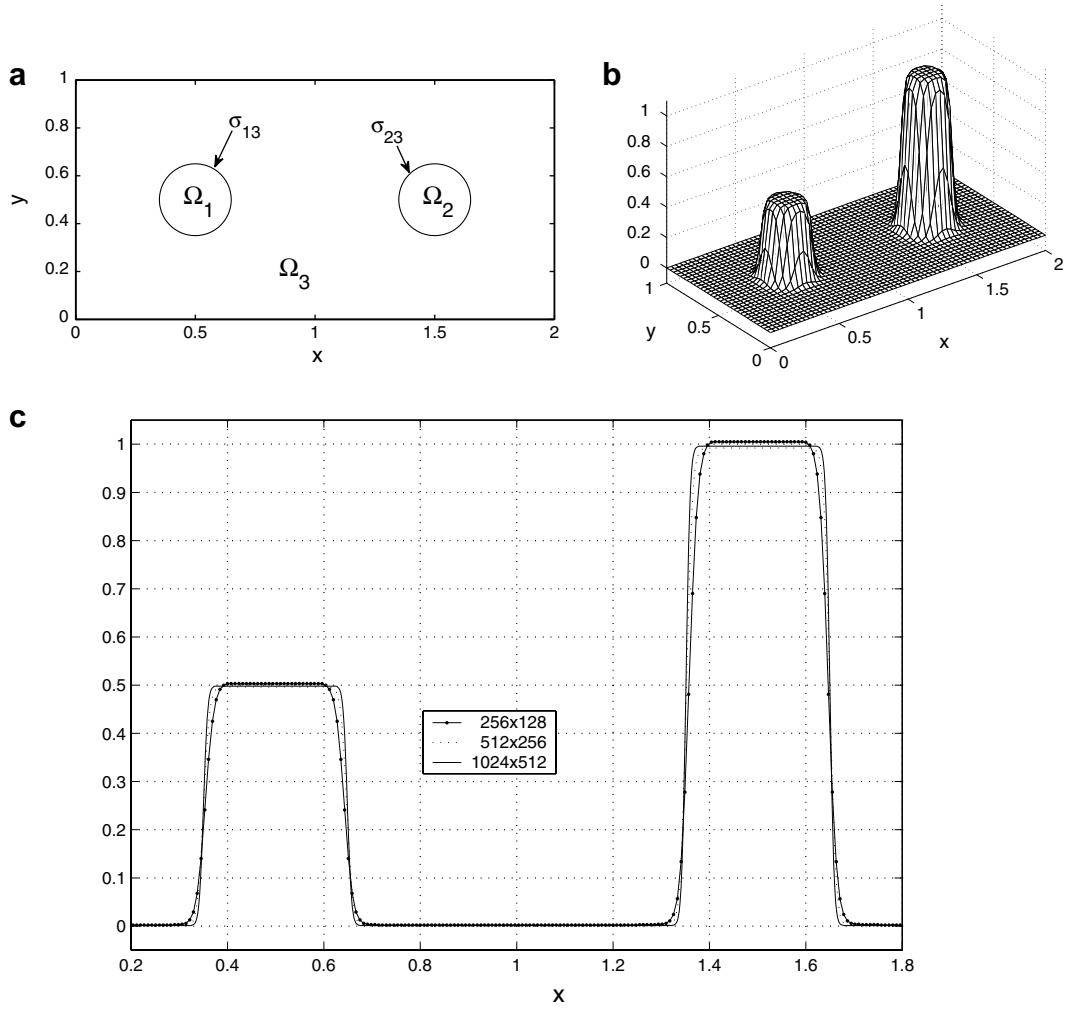

Fig. 7. (a) A schematic of two-dimensional drops, (b) the pressure field and (c) slice plots of the pressure field at $y = 0.5$ with three different mesh resolutions.

4.4. Liquid lens – contact angle

Following [29], we next investigated the spreading of a circular liquid lens (Fig. 8a) located at an interface between two other immiscible fluids. The initial condition is a circular droplet, Ω_2 (located at an interface between Ω_1 and Ω_3). The initial velocity was zero, i.e.,

$$c_1(x,y,0) = \max\left[0.5\left(1+\tanh\left(\frac{y-0.5}{2\sqrt{2}\epsilon}\right)\right) - c_2(x,y), 0\right],$$

$$c_2(x,y,0) = 0.5\left(1+\tanh\left(\frac{0.15-\sqrt{(x-0.5)^2+(y-0.5)^2}}{2\sqrt{2}\epsilon}\right)\right),$$

$$u(x,y,0) = v(x,y,0) = 0.$$

The computational domain was $\Omega = [0,1]\times[0,1]$ and the mesh size was 256×256. The fluid viscosities were matched $(\eta_1 = \eta_2 = \eta_3), Re = 60, We_2 = 60$, and $We_1 = We_3 = 36$.

In Fig. 8b, the evolution of the $c_2 = 1/2$ contour line is shown. In this case, $\epsilon = 0.006/\sqrt{2}$, $Pe = 10/\epsilon$, $h = 1/256$, and $\Delta t = 0.05h$ were used. As the droplet spread, it reached an equilibrium shape. The most deformed curve was the numerical steady-state. Theoretically, the shape of the steady-state drop is controlled by the three surface tension coefficients. The equilibrium three-phase contact angle is determined by

$$\frac{\sin\theta_1}{\sigma_{23}} = \frac{\sin\theta_2}{\sigma_{13}} = \frac{\sin\theta_3}{\sigma_{12}}.$$

The relationship between the lens area A, its length d (the distance between two triple junctions), and the contact angles θ_i (see Fig. 2) of the ith phase (Young's law) is

$$d = \left(\frac{2(\pi-\theta_1)-\sin(2(\pi-\theta_1))}{8A\sin^2(\pi-\theta_1)} + \frac{2(\pi-\theta_3)-\sin(2(\pi-\theta_3))}{8A\sin^2(\pi-\theta_3)}\right)^{-\frac{1}{2}}.$$

Thus, the accuracy of the steady lens shape can be measured by comparing the observed d with the analytical value. We found that there was very good agreement between the theoretical value, $d = 0.4596$ and the simulation result value, $d = 0.4539$.

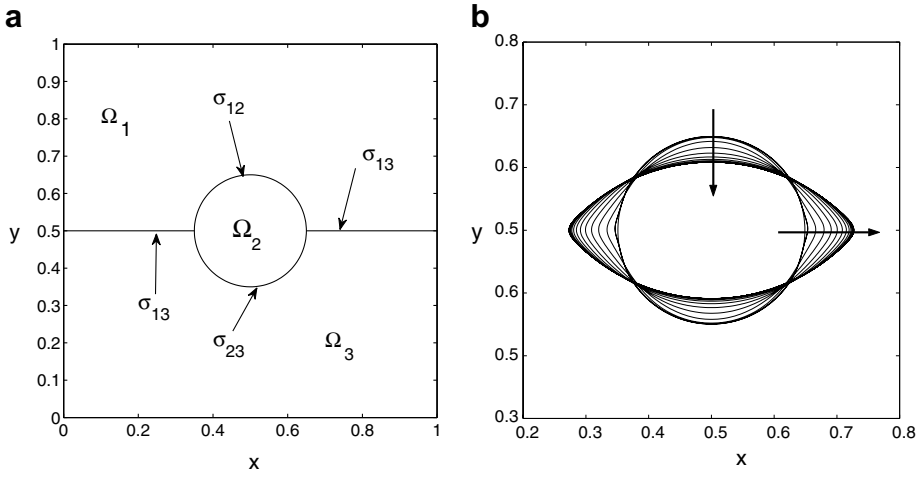

Fig. 8. (a) A schematic of the initial configuration: the upper fluid is in phase 1, the lower fluid is in phase 3, and the droplet is in phase 2. (b) The temporal evolution of the initial circular drop is shown for $We_2 = 60$ and $We_1 = We_3 = 36$. The arrow shows the direction of the evolution. The most deformed line is the steady shape.

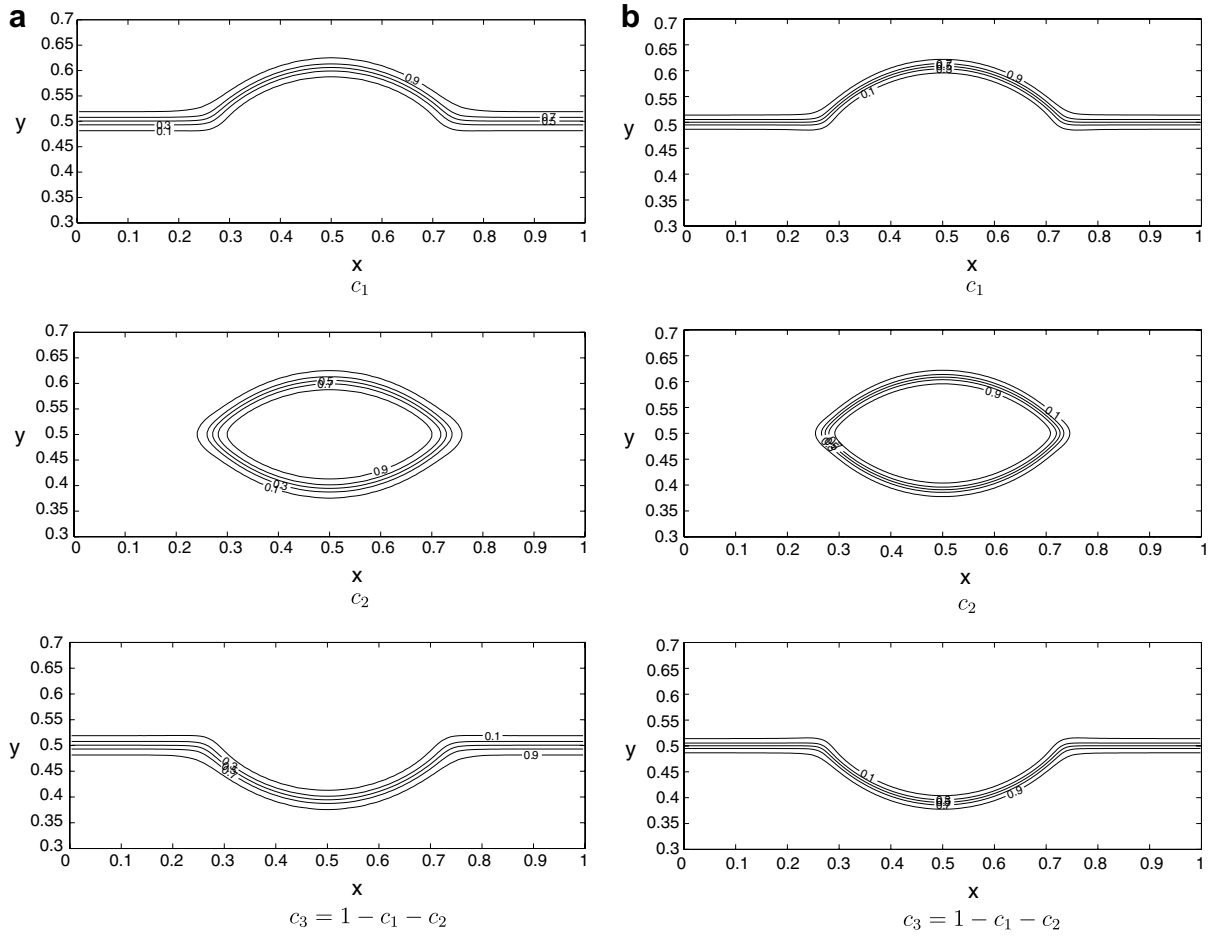

Fig. 9. Contour lines of concentration c_2 at the five levels $c_2 = 0.1, 0.3, 0.5, 0.7$, and 0.9. (a) and (b) are results with $\epsilon = 0.006$ on mesh size 128×128 and $\epsilon = 0.006/\sqrt{2}$ on mesh size 256×256, respectively.

In Fig. 9, we plot the final equilibrium stage with contour lines of each concentration c_i at the five levels $c_i = 0.1, 0.3, 0.5, 0.7$, and 0.9. Fig. 9a and b are results with $\epsilon = 0.006$ on a mesh size of 128×128 and $\epsilon = 0.006/\sqrt{2}$ on a mesh size of 256×256, respectively. Increasing resolution localizes the interfacial transition zone.

5. Conclusions

In this article, we proposed a new phase field model for the incompressible, immiscible ternary fluid flows with interfaces. The model consists of a Navier–Stokes equation with an extra surface tension term resulting from the presence of interfaces and a Cahn–Hilliard equation with the corresponding transport term. We used a recent chemical potential [5] and continuous surface tension force formulation [20], which has the capability to generalize to multi-component fluid flow models. We presented several illustrative numerical examples which exhibited various physical mechanisms of the model and demonstrated its robustness and versatility. In upcoming work, we will investigate the cases with more than three-component fluid flows with surface tension. In that work, we will generalize the continuous surface tension force formulation to multi-component (more than three) fluid flows.

Acknowledgement

This work was supported by the Korea Research Foundation Grant funded by the Korean Government (MOEHRD) (KRF-2006-C00225).

Appendix A. Ternary Cahn–Hilliard system with advection – a nonlinear multigrid method

In this section, we describe a nonlinear Full Approximation Storage (FAS) multigrid method to solve the nonlinear discrete system at the implicit time level. If the nonlinearity, $\mathbf{f}(\mathbf{c})$ in Eq. (19), is treated using one step of Newton's iteration, we obtain Gauss–Seidel–Newton relaxation. See the reference text [34] for additional details and the following notations. The convective CH Eqs. (18) and (19) can be written in the form $N(\mathbf{c}^{n+1}, \boldsymbol{\mu}^{n+\frac{1}{2}}) = (\boldsymbol{\phi}^n, \boldsymbol{\psi}^n)$, where the nonlinear system operator (N) is defined as

$$N(\mathbf{c}^{n+1}, \boldsymbol{\mu}^{n+\frac{1}{2}}) = \left(\frac{\mathbf{c}^{n+1}}{\Delta t} - \frac{1}{Pe}\Delta_d \boldsymbol{\mu}^{n+\frac{1}{2}}, \boldsymbol{\mu}^{n+\frac{1}{2}} - \frac{1}{2}\mathbf{f}(\mathbf{c}^{n+1}) + \frac{\epsilon^2}{2}\Delta_d \mathbf{c}^{n+1} \right)$$

and the source term is $(\boldsymbol{\phi}^n, \boldsymbol{\psi}^n) = \left(\frac{\mathbf{c}^n}{\Delta t} - (\mathbf{u}\cdot\nabla_d \mathbf{c})^n, \frac{1}{2}\mathbf{f}(\mathbf{c}^n) - \frac{\epsilon^2}{2}\Delta_d \mathbf{c}^n\right)$.

In the following description of one FAS cycle, we assume a sequence of grids Ω_k (Ω_{k-1} that is coarser than Ω_k by factor 2). Given the number v of pre- and post-smoothing relaxation sweeps, an iteration step for the nonlinear multigrid method using the V-cycle is formally written:

FAS multigrid cycle:

$$\left\{ \mathbf{c}_k^{m+1}, \boldsymbol{\mu}_k^{m+\frac{1}{2}} \right\} = \mathrm{FAScycle}(k, \mathbf{c}_k^m, \boldsymbol{\mu}_k^{m-\frac{1}{2}}, N_k, \boldsymbol{\phi}_k^n, \boldsymbol{\psi}_k^n, v)$$

on Ω_k grid.

That is, $\{\mathbf{c}_k^m, \boldsymbol{\mu}_k^{m-\frac{1}{2}}\}$ and $\{\mathbf{c}_k^{m+1}, \boldsymbol{\mu}_k^{m+\frac{1}{2}}\}$ are the approximations of $\{\mathbf{c}_k^{n+1}(x_i, y_j),\ \boldsymbol{\mu}_k^{n+\frac{1}{2}}(x_i, y_j)\}$ before and after an FAScycle. We set the initial guess, $\mathbf{c}_k^0 = \mathbf{c}_k^n$ and $\boldsymbol{\mu}_k^{-\frac{1}{2}} = \boldsymbol{\mu}_k^{n-\frac{1}{2}}$. Now, define the FAScycle.

Step 1 – Pre-smoothing:

$$\left\{ \bar{\mathbf{c}}_k^m, \bar{\boldsymbol{\mu}}_k^{m-\frac{1}{2}} \right\} = \mathrm{SMOOTH}^v(\mathbf{c}_k^m, \boldsymbol{\mu}_k^{m-\frac{1}{2}}, N_k, \boldsymbol{\phi}_k^n, \boldsymbol{\psi}_k^n) \quad \text{on } \Omega_k \text{ grid},$$

which means performing v smoothing steps with an initial approximation $\mathbf{c}_k^m, \boldsymbol{\mu}_k^{m-\frac{1}{2}}$, $\boldsymbol{\phi}_k^n, \boldsymbol{\psi}_k^n$, and the SMOOTH relaxation operator to get the approximation $\{\bar{\mathbf{c}}_k^m, \bar{\boldsymbol{\mu}}_k^{m-\frac{1}{2}}\}$. One SMOOTH relaxation operator step consists of solving the system (A.1) and (A.2) given below by the 4×4 matrix inversion for each ij. First, let us discretize Eq. (18).

$$\frac{\bar{\mathbf{c}}_{ij}^m}{\Delta t} + \frac{4}{h^2 Pe}\bar{\boldsymbol{\mu}}_{ij}^{m-\frac{1}{2}} = \boldsymbol{\phi}_{ij}^n + \frac{\boldsymbol{\mu}_{i+1,j}^{m-\frac{1}{2}} + \bar{\boldsymbol{\mu}}_{i-1,j}^{m-\frac{1}{2}} + \boldsymbol{\mu}_{i,j+1}^{m-\frac{1}{2}} + \bar{\boldsymbol{\mu}}_{i,j-1}^{m-\frac{1}{2}}}{h^2 Pe}. \tag{A.1}$$

Next, let us discretize Eq. (19). Since $\mathbf{f}(\bar{\mathbf{c}}_{ij}^m)$ is nonlinear with respect to $\bar{\mathbf{c}}_{ij}^m$, we linearize $\mathbf{f}(\bar{\mathbf{c}}_{ij}^m)$ at $\bar{\mathbf{c}}_{ij}^m$, i.e.,

$$\begin{aligned}
&\mathbf{f}(\bar{\mathbf{c}}_{ij}^m) \approx \mathbf{f}(\mathbf{c}_{ij}^m) + (\bar{\mathbf{c}}_{ij}^m - \mathbf{c}_{ij}^m)\frac{\partial \mathbf{f}(\mathbf{c}_{ij}^m)}{\partial \mathbf{c}}, \\
&\quad \text{where } \frac{\partial \mathbf{f}(\mathbf{c}_{ij}^m)}{\partial \mathbf{c}} = \begin{pmatrix} \frac{\partial f_1(\mathbf{c}_{ij}^m)}{\partial c_1} & \frac{\partial f_2(\mathbf{c}_{ij}^m)}{\partial c_1} \\ \frac{\partial f_1(\mathbf{c}_{ij}^m)}{\partial c_2} & \frac{\partial f_2(\mathbf{c}_{ij}^m)}{\partial c_2} \end{pmatrix}, \\
&-\bar{\mathbf{c}}_{ij}^m\left(\frac{\partial \mathbf{f}(\mathbf{c}_{ij}^m)}{2\partial \mathbf{c}} + \frac{2\epsilon^2}{h^2}\right) + \bar{\boldsymbol{\mu}}_{ij}^{m-\frac{1}{2}} \\
&\quad = \boldsymbol{\psi}_{ij}^n + \frac{1}{2}\mathbf{f}(\mathbf{c}_{ij}^m) - \mathbf{c}_{ij}^m\frac{\partial \mathbf{f}(\mathbf{c}_{ij}^m)}{2\partial \mathbf{c}} \\
&\qquad - \frac{\epsilon^2}{2h^2}(\mathbf{c}_{i+1,j}^m + \bar{\mathbf{c}}_{i-1,j}^m + \mathbf{c}_{i,j+1}^m + \bar{\mathbf{c}}_{i,j-1}^m).
\end{aligned} \tag{A.2}$$

Step 2 – Compute the defect:

$$(\overline{\mathbf{def}}_{1\,k}^m, \overline{\mathbf{def}}_{2\,k}^m) = (\boldsymbol{\phi}_k^n, \boldsymbol{\psi}_k^n) - N_k(\bar{\mathbf{c}}_k^m, \bar{\boldsymbol{\mu}}_k^{m-\frac{1}{2}}).$$

Step 3 – Restrict the defect and $\{\bar{\mathbf{c}}_k^m, \bar{\boldsymbol{\mu}}_k^{m-\frac{1}{2}}\}$*:*

$$(\overline{\mathbf{def}}_{1\,k-1}^m, \overline{\mathbf{def}}_{2\,k-1}^m, \bar{\mathbf{c}}_{k-1}^m, \bar{\boldsymbol{\mu}}_{k-1}^{m-\frac{1}{2}}) = I_k^{k-1}(\overline{\mathbf{def}}_{1\,k}^m, \overline{\mathbf{def}}_{2\,k}^m, \bar{\mathbf{c}}_k^m, \bar{\boldsymbol{\mu}}_k^{m-\frac{1}{2}}).$$

Step 4 – Compute the right-hand side:

$$(\boldsymbol{\phi}_{k-1}^n, \boldsymbol{\psi}_{k-1}^n) = (\overline{\mathbf{def}}_{1\,k-1}^m, \overline{\mathbf{def}}_2^m k-1) + N_{k-1}(\bar{\mathbf{c}}_{k-1}^m, \bar{\boldsymbol{\mu}}_{k-1}^{m-\frac{1}{2}}).$$

Step 5 – Compute an approximate solution $\{\hat{\mathbf{c}}_{k-1}^m, \hat{\boldsymbol{\mu}}_{k-1}^{m-\frac{1}{2}}\}$ *on* Ω_{k-1}*:*

$$N_{k-1}(\mathbf{c}_{k-1}^m, \boldsymbol{\mu}_{k-1}^{m-\frac{1}{2}}) = (\boldsymbol{\phi}_{k-1}^n, \boldsymbol{\psi}_{k-1}^n). \tag{A.3}$$

If $k = 1$, we explicitly invert a 4×4 matrix to obtain the solution. If $k > 1$, we solve Eq. (A.3) by performing a

FAS k-grid cycle using $\{\bar{\mathbf{c}}_{k-1}^{m}, \bar{\boldsymbol{\mu}}_{k-1}^{m-\frac{1}{2}}\}$ as an initial approximation:

$$\{\hat{\mathbf{c}}_{k-1}^{m}, \hat{\boldsymbol{\mu}}_{k-1}^{m-\frac{1}{2}}\} = \mathrm{FAScycle}(k-1, \bar{\mathbf{c}}_{k-1}^{m}, \bar{\boldsymbol{\mu}}_{k-1}^{m-\frac{1}{2}}, N_{k-1}, \boldsymbol{\phi}_{k-1}^{n}, \boldsymbol{\psi}_{k-1}^{n}, v).$$

Step 6 – Compute the coarse grid correction (CGC):

$$\hat{\mathbf{v}}_{k-1}^{m} = \hat{\mathbf{c}}_{k-1}^{m} - \bar{\mathbf{c}}_{k-1}^{m}, \hat{\mathbf{w}}_{k-1}^{m-\frac{1}{2}} = \hat{\boldsymbol{\mu}}_{k-1}^{m-\frac{1}{2}} - \bar{\boldsymbol{\mu}}_{k-1}^{m-\frac{1}{2}}.$$

Step 7 – Interpolate the correction:

$$(\hat{\mathbf{v}}_{k}^{m}, \hat{\mathbf{w}}_{k}^{m-\frac{1}{2}}) = I_{k-1}^{k}(\hat{\mathbf{v}}_{k-1}^{m}, \hat{\mathbf{w}}_{k-1}^{m-\frac{1}{2}}).$$

Step 8 – Compute the corrected approximation on Ω_k:

$$\mathbf{c}_{k}^{m,\text{after CGC}} = \bar{\mathbf{c}}_{k}^{m} + \hat{\mathbf{v}}_{k}^{m}, \boldsymbol{\mu}_{k}^{m-\frac{1}{2},\text{after CGC}} = \bar{\boldsymbol{\mu}}_{k}^{m-\frac{1}{2}} + \hat{\mathbf{w}}_{k}^{m-\frac{1}{2}}.$$

Step 9 – Post-smoothing:

$$\{\mathbf{c}_{k}^{m+1}, \boldsymbol{\mu}_{k}^{m+\frac{1}{2}}\} = \mathrm{SMOOTH}^{v}(\mathbf{c}_{k}^{m,\text{after CGC}}, \boldsymbol{\mu}_{k}^{m-\frac{1}{2},\text{after CGC}}, N_k, \boldsymbol{\phi}_{k}^{n}, \boldsymbol{\psi}_{k}^{n})$$

on Ω_k grid.

This completes the description of a nonlinear FAScycle.

References

[1] D. Anderson, G.B. McFadden, A.A. Wheeler, Diffuse interface methods in fluid mechanics, Ann. Rev. Fluid Mech. 30 (1998) 139–165.

[2] V.E. Badalassi, H.D. Ceniceros, S. Banerjee, Computation of multiphase systems with phase field models, J. Comput. Phys. 190 (2003) 371–397.

[3] A. Benichou, A. Aserin, N. Garti, Double emulsions stabilized by new molecular recognition hybrids of natural polymers, Polym. Adv. Technol. 13 (2002) 1019–1031.

[4] J.F. Blowey, M.I.M. Copetti, C.M. Elliott, Numerical analysis of a model for phase separation of a multi-component alloy, IMA J. Numer. Anal. 16 (1996) 111–139.

[5] F. Boyer, C. Lapuerta, Study of a three component Cahn–Hilliard flow model, M2AN 40 (4) (2006) 653–687.

[6] J.U. Brackbill, D.B. Kothe, C. Zemach, A continuum method for modeling surface tension, J. Comput. Phys. 100 (1992) 335–354.

[7] A.F. Brodin, D.R. Kavaliunas, S.G. Frank, Prolonged drug release from multiple emulsions, Acta Pharm. Suec. 15 (1) (1978) 1–12.

[8] A.J. Chorin, A numerical method for solving incompressible viscous flow problems, J. Comput. Phys. 2 (1967) 12–26.

[9] Y.C. Chang, T.Y. Hou, B. Merriman, S. Osher, A level set formulation of Eulerian interface capturing methods for incompressible fluid flows, J. Comput. Phys. 124 (1996) 449–464.

[10] R. Chella, J. Viñals, Mixing of a two-phase fluid by cavity flow, Phys. Rev. E 53 (1996) 3832–3840.

[11] L.Q. Chen, A computer simulation technique for spinodal decomposition and ordering in ternary systems, Scr. Metall. Mater. 29 (5) (1993) 683–688.

[12] Y.H. Cho, J. Park, Evaluation of process parameters in the O/W/O multiple emulsion method for flavor encapsulation, J. Food Sci. 68 (2003) 534–538.

[13] M.I.M. Copetti, Numerical experiments of phase separation in ternary mixtures, Math. Comput. Simul. 52 (1) (2000) 41–51.

[14] M. Francois, W. Shyy, Computations of drop dynamics with the immersed boundary method, part 1: numerical algorithm and buoyancy-induced effect, Numer. Heat Transfer, Part B 44 (2003) 101–118.

[15] D. Gao, N.B. Morley, V. Dhir, Numerical simulation of wavy falling film flow using VOF method, J. Comput. Phys. 192 (2003) 624–642.

[16] D. Gueyffier, J. Li, A. Nadim, R. Scardovelli, S. Zaleski, Volume-of-fluid interface tracking with smoothed surface stress methods for three-dimensional flows, J. Comput. Phys. 152 (1999) 423–456.

[17] H. Garcke, B. Nestler, B. Stoth, On anisotropic order parameter models for multi-phase systems and their sharp interface limits, Physica D 115 (1998) 87–108.

[18] F. Harlow, J.E. Welch, Numerical calculations of time dependent viscous incompressible flow with free surface, Phys. Fluids 8 (1965) 2182–2189.

[19] D. Jacqmin, Contact-line dynamics of a diffuse fluid interface, J. Fluid Mech. 402 (2000) 57–88.

[20] J.S. Kim, A continuous surface tension force formulation for diffuse-interface models, J. Comput. Phys. 204 (2) (2005) 784–804.

[21] J.S. Kim, A generalized continuous surface tension force formulation for phase field models for immiscible multi-component fluid flows, in preparation.

[22] J.S. Kim, J.S. Lowengrub, Phase field modeling and simulation of three-phase flows, Interfaces Free Bound. 7 (2005) 435–466.

[23] J.S. Kim, J.S. Lowengrub, Interfaces and Multicomponent Fluids, Encyclopedia of Mathematical Physics, Elsevier, 2006.

[24] E.B. Nauman, D.Q. He, Morphology predictions for ternary polymer blends undergoing spinodal decomposition, Polymer 35 (1994) 2243–2255.

[25] D.A. Porter, K.E. Easterling, Phase Transformations in Metals and Alloys, van Nostrand Reinhold, 1993.

[26] Y.Y. Renardy, M. Renardy, V. Cristini, A new volume-of-fluid formation for surfactants and simulations of drop deformation under shear at a low viscosity ratio, Eur. J. Mech. B/Fluids 21 (2002) 49–59.

[27] J.A. Sethian, P. Smereka, Level set methods for fluid interfaces, Annu. Rev. Fluid Mech. (35) (2003) 341–372.

[28] C.W. Shu, S. Osher, Efficient implementation of essentially non-oscillatory shock capturing schemes II, J. Comput. Phys. 83 (1989) 32–78.

[29] K.A. Smith, F.J. Solis, D.L. Chopp, A projection method for motion of triple junctions by levels sets, Interfaces Free Bound 4 (2002) 263–276.

[30] M. Sussman, A.S. Almgren, J.B. Bell, P. Colella, L.H. Howell, M.L. Welcome, An adaptive level set approach for incompressible two-phase flows, J. Comput. Phys. 148 (1) (1999) 81–124.

[31] Y. Sun, C. Beckermann, Diffuse interface modeling of two-phase flows based on averaging: mass and momentum equations, Physica D 198 (2004) 281–308.

[32] M. Sussman, P. Smereka, S.J. Osher, A level set method for computing solutions to incompressible two-phase flow, J. Comput. Phys. 114 (1994) 146–159.

[33] H. Tang, L.C. Wrobel, Z. Fan, Tracking of immiscible interfaces in multiple-material mixing processes, Comp. Mater. Sci. 29 (2004) 103–118.

[34] U. Trottenberg, C. Oosterlee, A. Schüller, Multigrid, Academic Press, 2001.

[35] A.S. Utada, E. Lorenceau, D.R. Link, P.D. Kaplan, H.A. Stone, D.A. Weitz, Monodisperse double emulsions generated from a microcapillary device, Science 308 (5721) (2005) 537–541.